Changes of Crystal Structure and Electrical Properties with Film Thickness and Zr/(Zr+Ti) Ratio for Epitaxial Pb(Zr,Ti)O$_3$ Films Grown on (100)$_c$SrRuO$_3$//(100)SrTiO$_3$ Substrates by Metalorganic Chemical Vapor Deposition

Mohamed-Tahar Chentir[1], Hitoshi Morioka[1,2],
Yoshitaka Ehara[1], Keisuke Saito[2], Shintaro Yokoyama[1],
Takahiro Oikawa[1] and Hiroshi Funakubo[1]
[1]Tokyo Institute of Technology, Department of Innovative and Engineered Materials,
Interdisciplinary Graduate School of Science and Engineering
[2]Application Laboratory, Bruker AXS
Japan

1. Introduction

Lead zirconium titanate, Pb(Zr,Ti)O$_3$ [PZT], have been intensively studied for various ferroelectric applications, and have a renewal interest due to their promising application for microelectromechanical systems (MEMS) because of their outstanding ferroelectric and piezoelectric properties. Remanent polarization (P_r) is the not only most fundamental parameter but also the practical importance for real applications to achieve high density devices. Spontaneous polarization (P_S) is the expected maximum P_r value of the materials that depend on the composition, orientation and the crystallinity of Pb(Zr,Ti)O$_3$. Thus, in an academic point of view, lots of efforts have been made to investigate P_S value. However, PZT crystals with single domain are hard to be obtained, inducing a lack of direct characterization of P_S values using PZT single crystal. This situation is due to $c/a/c/a$ polydomain structure of PZT, where a domain and c domain are respective (100) and (001) oriented domains. This domain structure is the result of relaxation process of stress induced under the growth process of PZT.

To achieve this purpose, we switch our idea from growth of the bulky single crystal to epitaxial films with polar axis orientation. In addition, a comprehensive and systematic characterization of ferroelectric properties of PZT films with different volume fraction of polar-axis-oriented domain is investigated.

This chapter investigates the thickness and Zr/(Zr+Ti) ratio dependencies of domain structure and ferroelectric properties, and correlates physical properties, namely lattice

parameters and the volume fractions of the domains, as well as the electrical properties such as P_r and P_S.

2. Experimental

PZT thin films were grown on $(100)_c SrRuO_3//(100)SrTiO_3$ substrates at 540°C by pulsed-metal organic chemical vapor deposition (MOCVD) from $Pb(C_{11}H_{19}O_2)_2$ - $Zr(O·t-C_4H_9)_4$ - $Ti(O·i-C_3H_7)_4$ - O_2 system (Nagashima et al., 2001). Epitaxial $(100)_c SrRuO_3$ thin films used for bottom electrode layers were grown on $(100)SrTiO_3$ substrates by MOCVD (Okuda et al., 2000). The $Zr/(Zr+Ti)$ ratio and the film thickness of PZT films were controlled by the input gas concentration of the source gases and the deposition time, respectively. In this work, we studied PZT films having thickness ranging from 50 to 250 nm.

The orientation of the deposited films was analyzed by high-resolution X-Ray Diffraction (XRD) using a four-axis diffractometer (PANalytical X'Pert MRD). The high-resolution XRD reciprocal space mapping (HRXRD-RSM) was also employed for more detail analysis of crystal structure (orientation, in-plane and out-of-plane lattice parameters, and the internal axial angle) and estimating the relative volume fraction of the *c*-domain in tetragonal phase (Saito et al., 2003a).

Electron-beam deposition was used to deposit 100 μmϕ Pt top electrodes for the electrical property characterization of PZT films. The polarization – electric-field (*P* - *E*) hysteresis loops of the as-deposited films were measured at 20 Hz by the ferroelectric tester using pulsed rectangular wave (Radiant Technologies RT6000HVS and TOYO Corporation FCE-1).

3. Results and discussion

In this section, we demonstrate, first of all, film thickness dependency of the crystal structure of PZT films. We show that polar-axis-oriented films were obtained at very thin films region. Then, we detail the $Zr/(Zr+Ti)$ ratio dependency of the domain structure. For this purpose, we will compare crystal structure evolution as a function of the $Zr/(Zr+Ti)$ ratio at two thicknesses, 50 and 250 nm. This comparative study aims to emphasis the role of the $Zr/(Zr+Ti)$ ratio in PZT film as well as the thickness dependency, discussed in first instance.

Finally, we will cross check the up mentioned results by monitoring the evolution of electrical properties versus thickness and the $Zr/(Zr+Ti)$ ratio in the films. We will synthesis these data by identifying the linear relationship between the square of spontaneous polarization (P_s^2) and tetragonal distortion ($1-c/a$).

Nevertheless, prior to proceeding to this characterization, it is important to check the epitaxial relationship between the bottom electrode and PZT films.

Indeed, it must be kept in mind that the framework of this study is the fundamental understanding of the impact of crystal structure change on the electrical properties, and polycrystalline films might induce measurement artefacts. The epitaxial growth of PZT films on $(100)SrRuO_3//(100)SrTiO_3$ substrates was ascertained by High Resolution Transmittance Electron Microscopy (HRTEM) as presented on Fig. 1(a).

Indeed, Fig. 1(a) shows a cross-sectional TEM image of 50 nm thick PZT(35/65) film. It presents smooth interfaces. Fig. 1(b) reveals atomically sharp interface between PZT and

SrRuO$_3$ bottom electrode. Moreover, this latter figure shows clearly a coherent epitaxial relationship at PZT/SrRuO$_3$ interface.
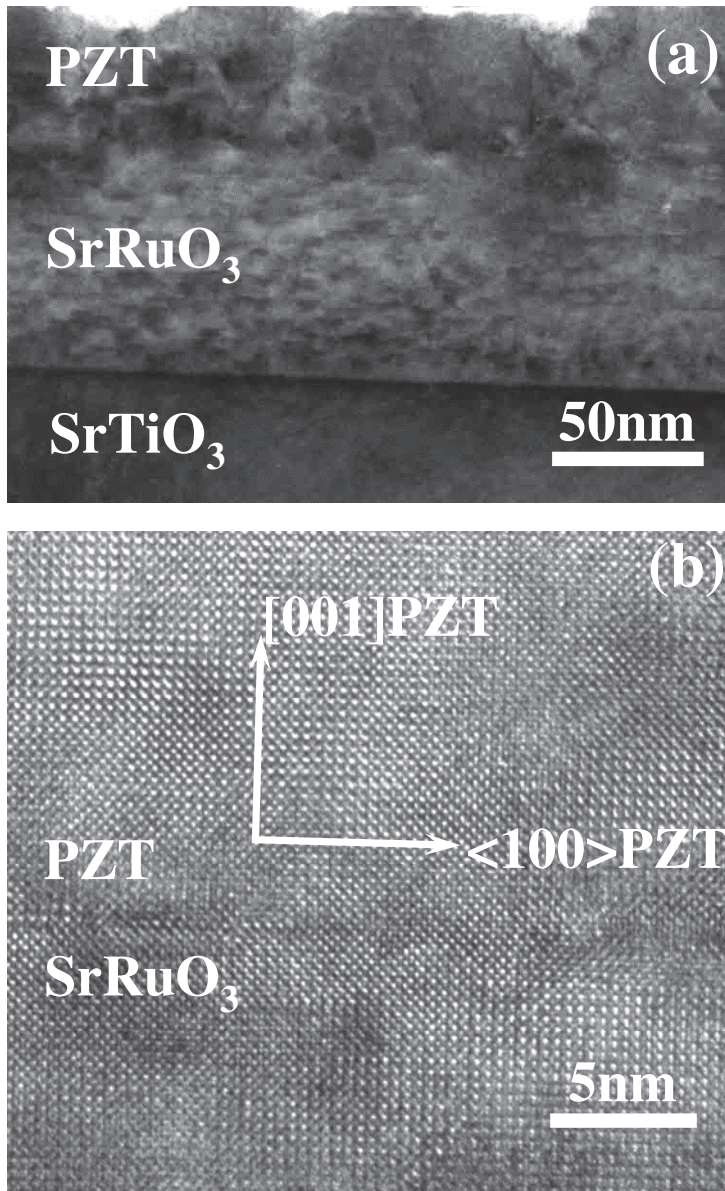

Fig. 1. Cross sectional TEM imaging of PZT(35/65)/SrRuO$_3$/SrTiO$_3$ (a). HRTEM of PZT-SrRuO$_3$ interface reveals a coherent epitaxial growth of PZT on SrRuO$_3$ bottom electrode (b).

3.1 Evolution of domain structure versus film thickness

For this part of our investigation, we chose to characterize PZT films with the Zr/(Zr+Ti) ratio of 0.35 that have a tetragonal symmetry. Fig. 2 presents XRD plots for the 2θ angle range of 2θ = 40 - 50°. On this figure we notice that PZT *200* peak decreases with decreasingly film thickness. This phenomenon might have two possibilities: one is the change of the tilting angle against the surface normal direction. The other is the change of domain structure from the mixed domain structure of *a* and *c* domains to fully *c*-domain oriented film with decreasing film thickness.

Hence, using XRD-RSM technique (Fig. 3), we could monitor *c*-domain volume fraction $[V_c = V_{(001)}/(V_{(100)} + V_{(001)})]$ as a function of film thickness as shown in Fig. 4. On this figure, we notice that films having thicknesses under around 75 nm, are perfect polar axis-oriented films. Over this threshold, *c*-domain volume fraction decreases almost linearly with increasing thickness up to 230 nm..
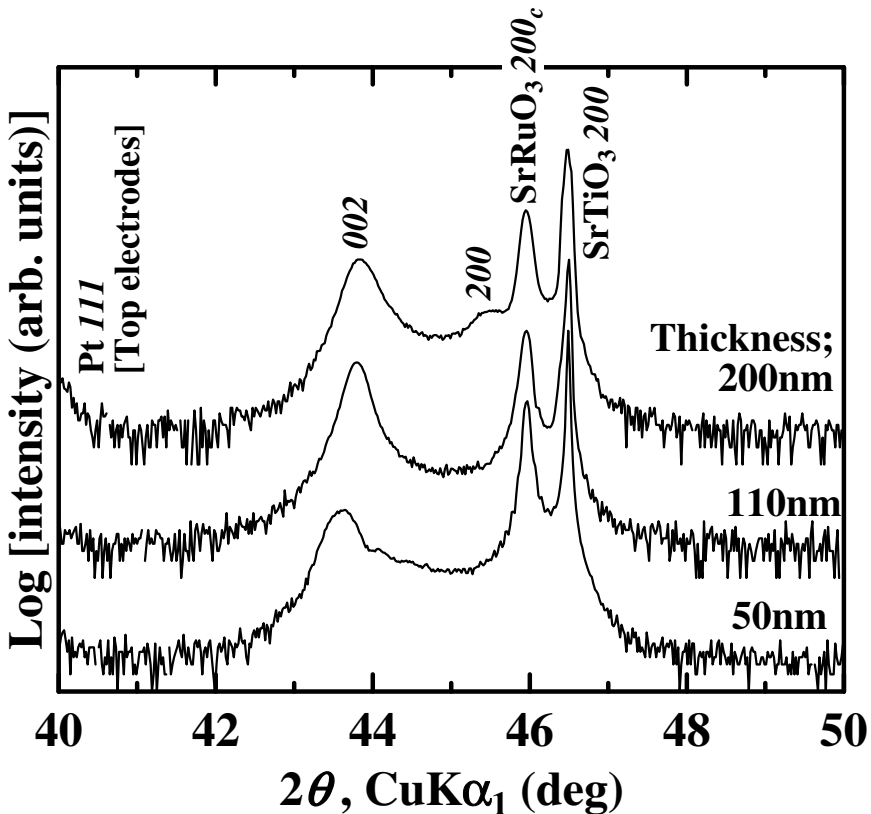

Fig. 2. XRD plots of PZT(35/65) films having thicknesses ranging from 50 to 200 nm. As film thickness increases, PZT *200* peak appears indicating the coexistence of *a*-domain with *c*-domains.
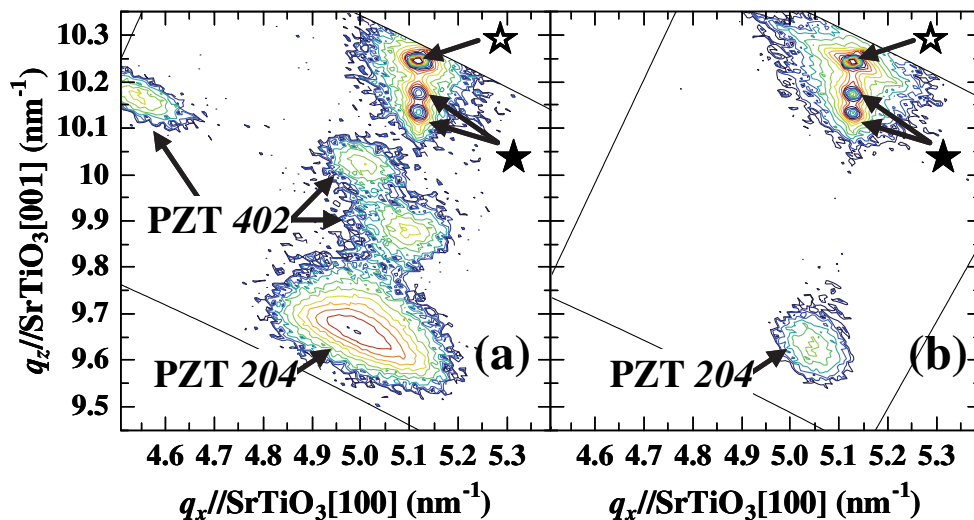
Fig. 3. XRD-RSM of PZT(35/65) films having thicknesses of (a) 250 nm and (b) 50 nm.
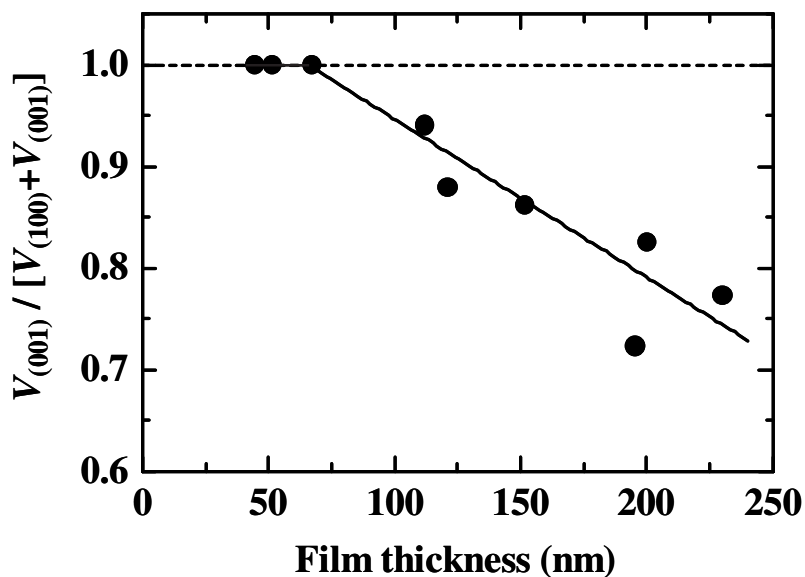SrTiO₃ *204* spot (☆) and splitted sport of SrRuO₃ *204* (★) are also illustrated.

Fig. 4. Evolution of *c*-domain volume fraction [$V_c = V_{(001)}/(V_{(100)} + V_{(001)})$] as a function of PZT
thickness in the case of PZT(35/65) films.

Finally, we checked strain condition when film thickness decrease in the case of PZT(35/65) material. For this purpose, we calculated the both in-plan ($a_{//}$ and $c_{//}$) and out-of-plan ($a_\perp$ and $c_\perp$) lattice parameters as a function of PZT film thickness (Fig. 5). On this figure, we also indicate SrTiO$_3$ lattice parameter (a= 0.3905 nm) as well as unstrained PZT(35/65) lattice parameters extracted from powder data (a = 0.398 nm and c = 0.413 nm) (Shirane & Suzuki, 1952). It is interesting to notice that in-plan and out-of-plan lattice parameters are almost constant regardless of the film thickness range studied in this work, demonstrating almost relaxed unit cells due to the large lattice mismatch between Pb(Zr$_{0.35}$Ti$_{0.65}$)O$_3$ films and SrTiO$_3$ substrates.
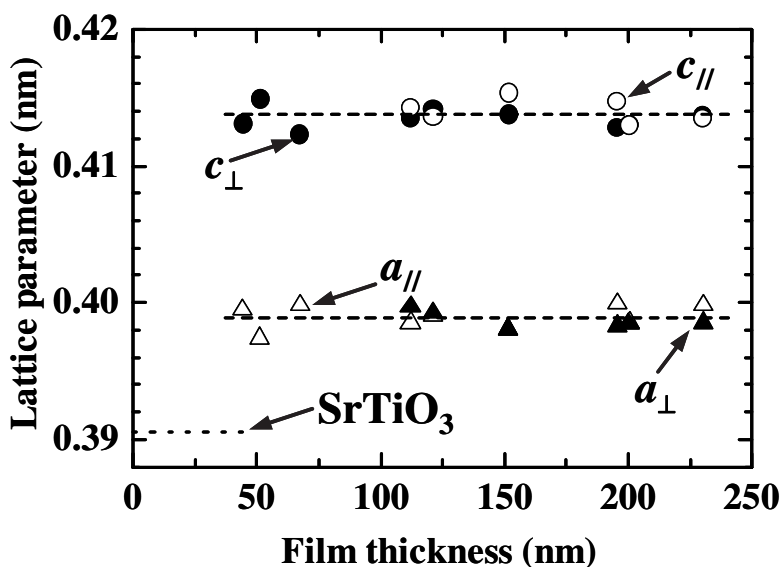

Fig. 5. In-plane and out-of-plane lattice parameters as function of film thickness in the case of Pb(Zr$_{0.35}$Ti$_{0.65}$)O$_3$ films.

3.2 Domain structure evolution versus film composition

Fig. 6 presents X-ray diffraction diagrams of PZT films having 50 and 250 nm in thickness with various Zr/(Zr+Ti) ratio. All films are found to have (100) and/or (001) orientations regardless of the film thickness and Zr/(Zr+Ti) ratio. Epitaxial relationship of (001)/(100)PZT //(100)$_c$SrRuO$_3$//(100) SrTiO$_3$ was ascertained by XRD pole figure measurement for all films. Figures 7(a) - (f) summarize a- and c-axes lattice parameters, tetragonality (c/a ratio) and the internal angles (α), and the unit cell volume as a function of the Zr/(Zr+Ti) ratio for 50 and 250 nm-thick PZT films. Reported data by Shirane et al. for PZT powder are also presented on these figures (Shirane & Suzuki, 1952).

As shown in Fig. 7, our experimental data are in good agreement with reported data of powders. However, an intermediate region can easily be observed in the 250 nm thick sample. This region could be related to the coexistence of both tetragonal and rhombohedral phases (Morioka et al. 2004a), suggesting a strain relaxation mechanism at this thickness (Morioka et al. 2004b).
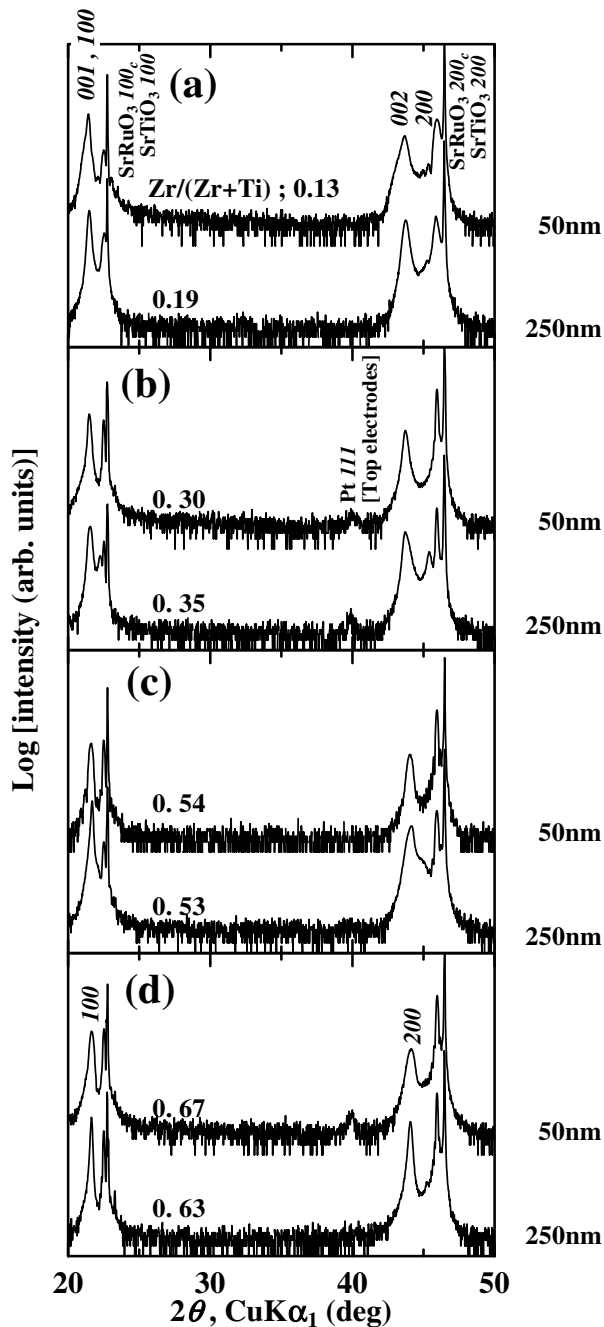
Fig. 6. XRD ω-2θ diagrams of PZT films having 50 and 250 nm in thickness and different Zr/(Zr+Ti) ratio: from small Zr/(Zr+Ti) ratio (a) to large Zr/(Zr+Ti) ratio (d).
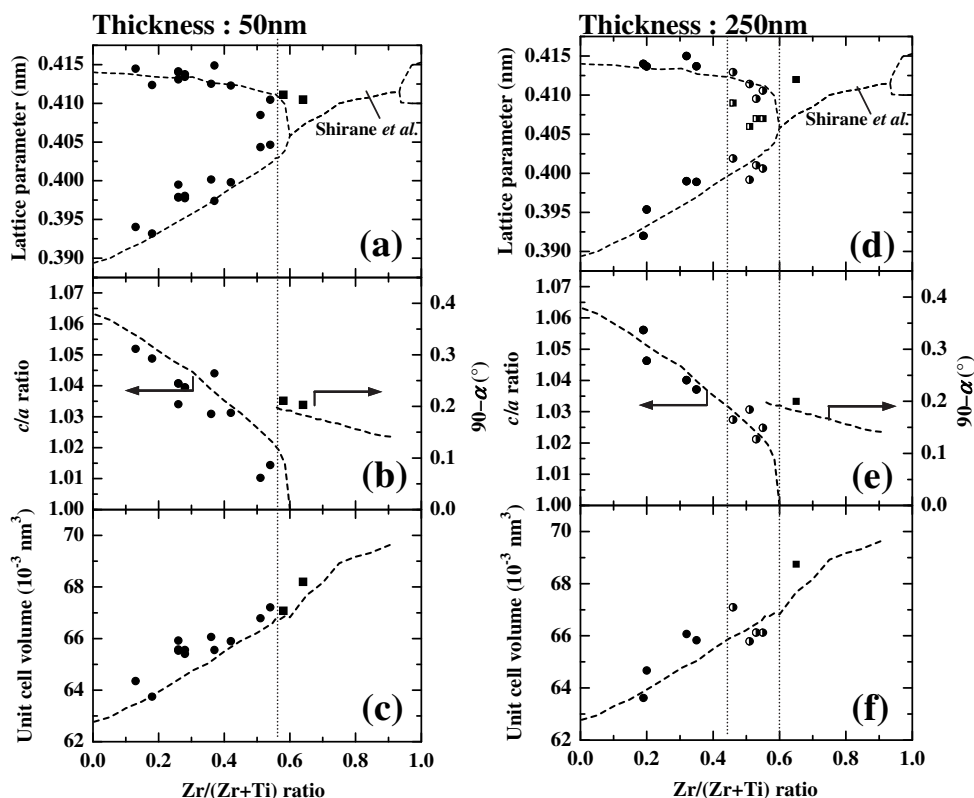
Fig. 7. Lattice parameters (a, d), tetragonality, c/a ratio, and the internal angles and (b, e), and unit cell volume (c, f) as a function of Zr/(Zr+Ti) ratio for (a)-(c) 50 and (d)-(f) 250 nm thick films. Dashed lines are powder data reported by Shirane et al (Shirane & Suzuki, 1952).

The c-domain relative volume fractions, V_c, are shown in Fig. 8 as a function of the Zr/(Zr+Ti) ratio. These values are obtained from HRXRD-RSM characterization reported elsewhere (Morioka et al. 2004a).

On this figure we notice that the 50 nm thick Films are fully polar axis-oriented films, (001) orientation, regardless of the Zr/(Zr+Ti) ratio up to 54% (Fig. 8(a)). On the other hand, V_c decreased with increasing PZT film thickness. Indeed, we notice for the 250 nm thick films (Fig. 8(b)) that V_c is about 70% up to Zr/(Zr+Ti) = 0.45. In the intermediate region, V_c fluctuates between 55 and 75% due to the experimental errors induced by the tetragonal and rhombohedral duplicated peaks (Saito et al., 2003b). This result is totally coherent with our previous results showing the domain structure simplification with decreasing PZT film thickness. The structure domain simplification from coexisting a- and c-domains to fully polar axis orientation is supported by the compressive stress appearing at very thin deposited films (Morioka et al., 2003; Morioka et al., 2009). This compressive stress is induced by the lattice misfit stress and thermal stress due to the mismatches of lattice parameters and thermal expansion coefficients between PZT films and SrTiO$_3$ substrates, respectively.
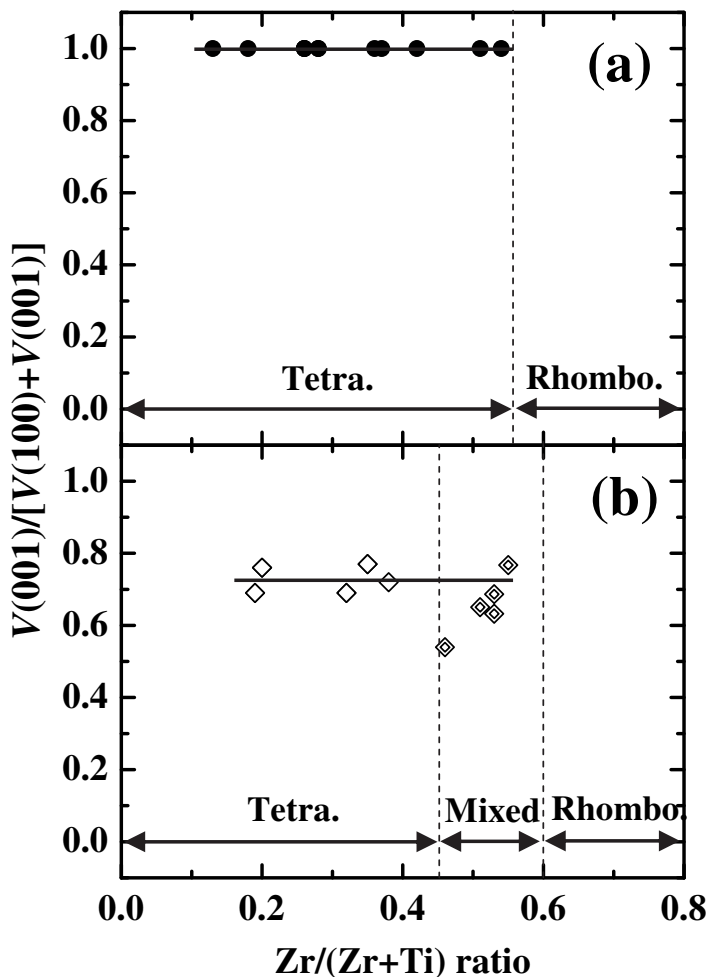
Fig. 8. c-domain volume fraction, V_c, measured from HRXRD-RSM data (Morioka et al.
2004a) for (a) 50 and (b) 250 nm thick PZT films.

3.3 Electrical characterization

Fig. 9 shows the leakage current density as a function of applied electric field for 50 and 250
nm thick PZT films with various Zr/(Zr+Ti) ratio. We notice that PZT thickness and
Zr/(Zr+Ti) ratio influences leakage current density. Indeed, below 20% of Zr/(Zr+Ti) ratio,
the 250 nm thick films show higher current density than 50 nm thick sample [see Fig. 9(a)].
Increasing Zr/(Zr+Ti) ratio in films lead to a decrease of the leakage current density level in
the 250 nm thick PZT films from above 10^{-3} A/cm² to 10^{-6} A/cm² at an electric field of
100 kV/cm for Zr/(Zr+Ti) ratio ranging from 0.19 and 0.63 respectively.
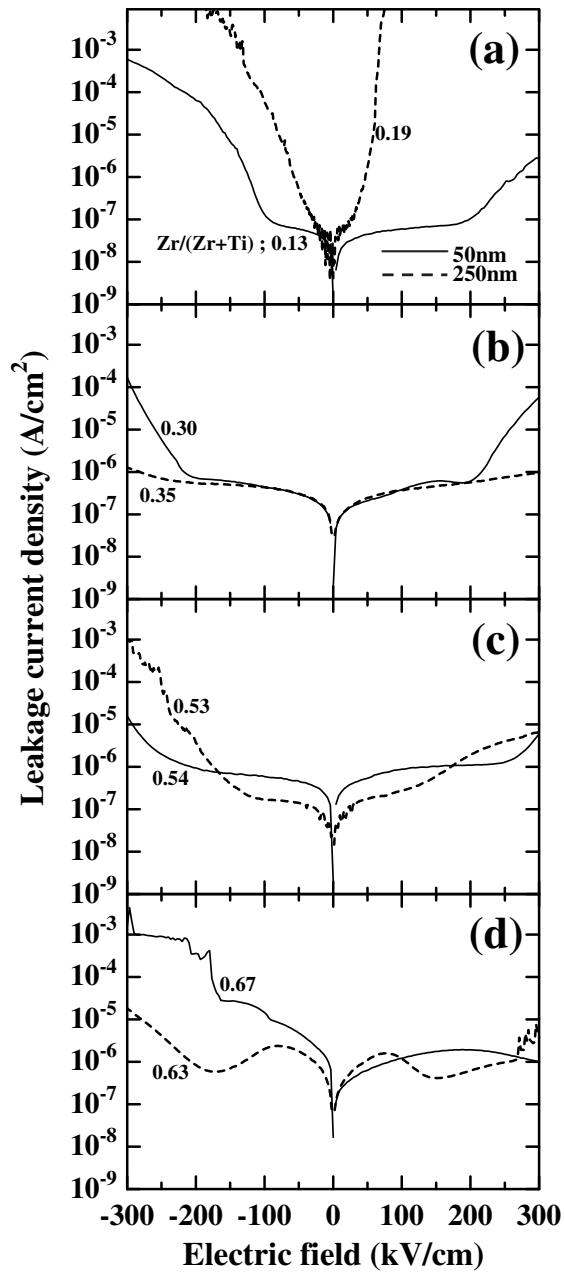
Fig. 9. Leakage current density as a function of electric filed for 50 nm thick (plain line) and 250 nm thick (dotted line) PZT thin films with different Zr/(Zr+Ti) ratio: from small Zr/(Zr+Ti) ratio (a) to large Zr/(Zr+Ti) ratio (d).

On the other hand, the 50 nm thick PZT film show a relatively low leakage current level oscillating between 10^{-7} and 10^{-5} A/cm^2 at an electric field of 100 kV/cm, independently from the Zr/(Zr+Ti) ratio. These results are coherent with reported data (Shiosaki, 1995; Oikawa et al., 2002). Indeed, it has been shown that PZT films with low Zr/(Zr+Ti) ratio present typically larger leakage current density compared to that of films with large Zr/(Zr+Ti) ratio (Shiosaki, 1995). While it has been revealed (Oikawa et al., 2002) that Sr and/or Ru diffusion into PZT might create a conductive path, which is in good agreement with our results because a longer deposition time could induce a large amount of Sr and/or Ru diffusion into the bottom electrode.

Fig. 10 summarizes the polarization - electric field (*P* - *E*) relationships for films with various Zr/(Zr+Ti) ratio and film thickness.
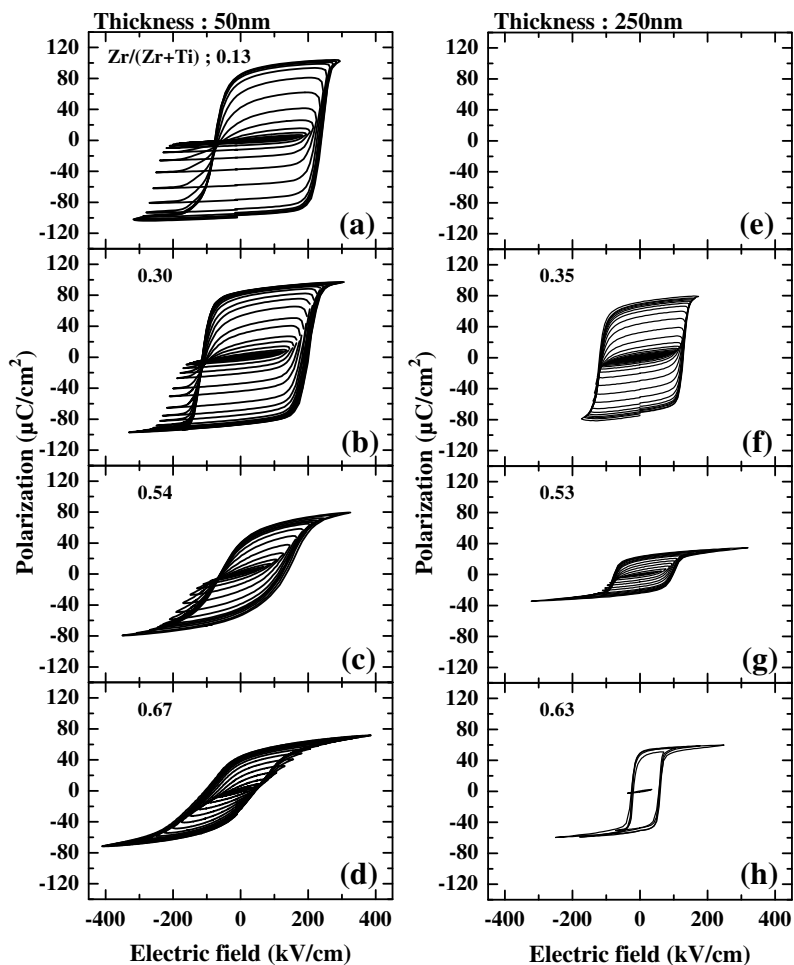

Fig. 10 Polarization - electric field (*P* - *E*) relationships for films with various Zr/(Zr+Ti) ratio and film thickness. from 50 nm thick films [(a)-(d)] and 250 nm thick films [(e) - (h)].
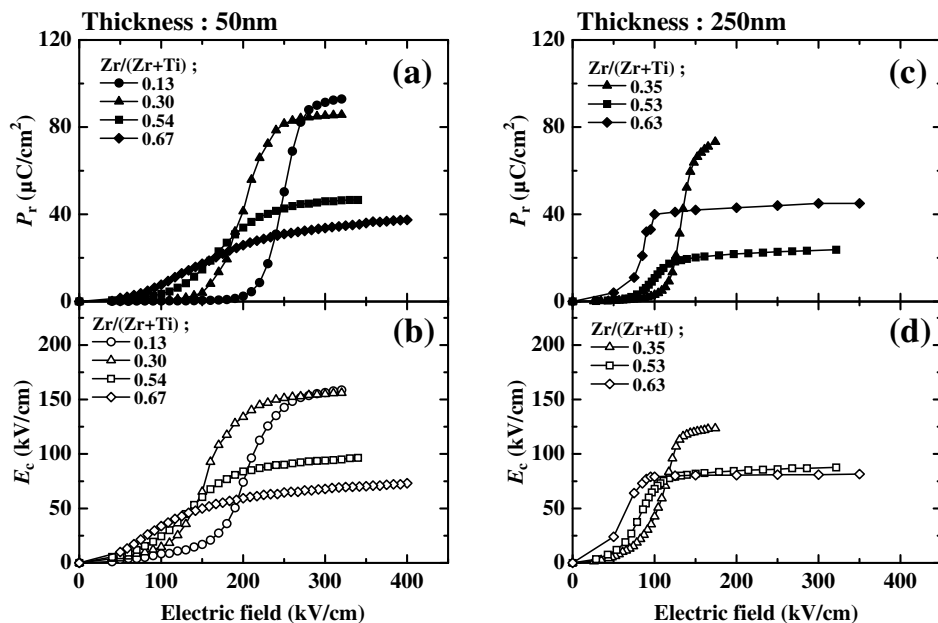
Fig. 11. Saturation properties of P_r and E_c values against the maximum applied electric filed for 50 nm [(a), (b)] and 250nm [(c), (d)] PZT films having various Zr/(Zr+Ti) ratio content.

Notice that the 250 nm thick film with Zr/(Zr+Ti)=0.19 showed high leakage current level that cannot display P - E hysterisis loops from the PZT films [Fig. 9(a)]. However, others showed P - E hysteresis loops originated to the ferroelectricity. Good saturation properties of Pr and the coercive field (Ec) against the maximum electric filed are confirmed for both of 50 nm and 250 nm thick films.

We notice on these figures that fully polar axis oriented [(001)-oriented] films with 50 nm in thickness exhibit larger P_r values than 250 nm PZT films with the coexistence of (100) and (001) orientations. This result is coherent if we consider the difference in the relative volume fraction of the c-domain in the latter samples. However, the differences in domain structure between the two thickness of the present samples remains and issue to fix for a good comparative analysis.

To get insight into this issue, we calculated the spontaneous polarization (P_{sat}) from P_r/V_c, calibrated P_r value by the c-domain volume fraction, V_c, assuming that the 90° a-domain do not switch under an external electric field. The results are summarized in Fig. 12.

On this figure, P_r values extracted from 50 nm-thick films are presented with closed diamonds, while open diamonds represents P_r values of 250 nm-thick films. By way of comparison, we included on Fig. 12, reported data for the 100% c-axis-oriented Pb(Zr$_{0.5}$Ti$_{0.5}$)O$_3$ film by Ishida et al. (square plot) (Ishida et al., 2002) and also theoretical calculated data of P_{sat} against the Zr/(Zr+Ti) ratio reported by Haun et al. (dashed line) (Haune et al., 1989).

We notice that the estimated P_{sat} value in the present study is larger than reported data. However, our results have the same trend as predicted by theoretical calculations.

A good explanation of this latter result might be given by getting insight into the relationship linking tetragonality (c/a) to spontaneous polarization (P_{sat}).
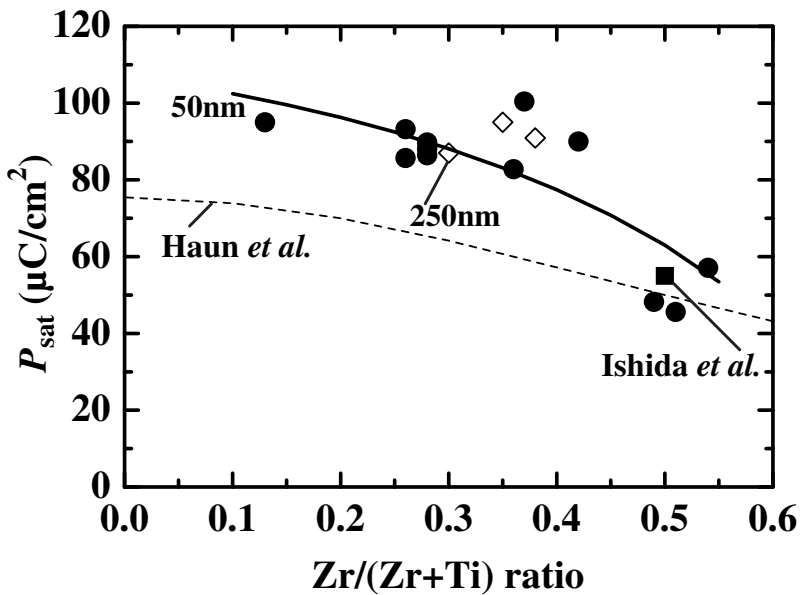
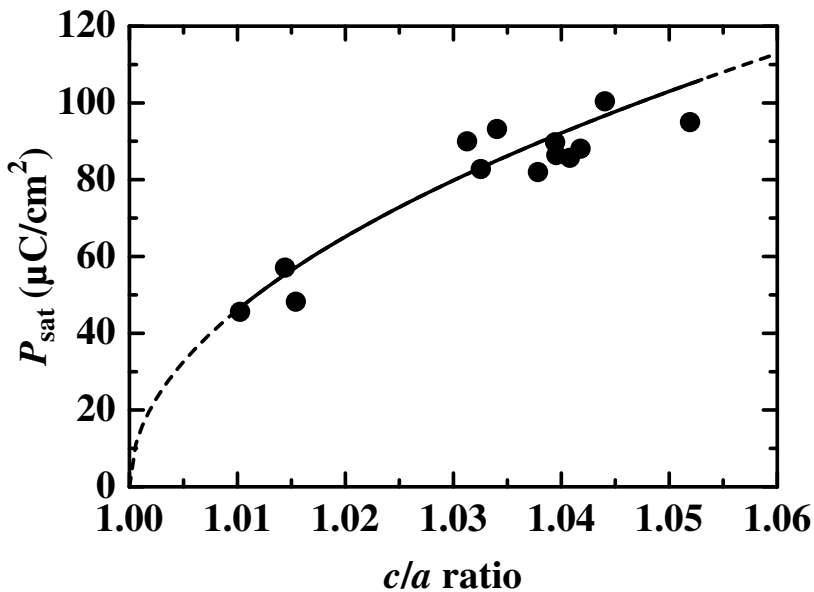Fig. 12. Estimated P_{sat} as a function of Zr/(Zr+Ti) ratio in films.

Fig. 13. Relationship between P_{sat} and the c/a ratio of PZT films.

Indeed, the unit cell distortion inducing P_{sat} might be related to cell parameters by the following equation (Joan & Shirane, 1992):

$$Q \cdot P_{sat}^2 = \frac{c}{a} - 1 \tag{1}$$

where, Q represents the apparent electrostrictive coefficient.

To highlight this relationship, we gathered data presented on Figures 7(b) and (e) and Fig. 12 on the same chart, as shown in Fig. 13:

Our data seem to be in agreement with the quadratic form presented in equation (1) linking P_{sat} to unit cell tetragonality, c/a ratio. In a previous article we could emphasis that our estimated electrostrictive coefficient, Q, is $Q = 0.049$ m^4/C^2

We also characterized the relative dielectric constant (ε_r) versus Zr/(Zr+Ti) ratio as well as thickness dependency. These results are presented on Fig. 14. On this figure, we notice that both thicknesses considered in this study respect the same ε_r tendency with regards to Zr content. Indeed, ε_r increases with increasing Zr/(Zr+Ti) ratio.

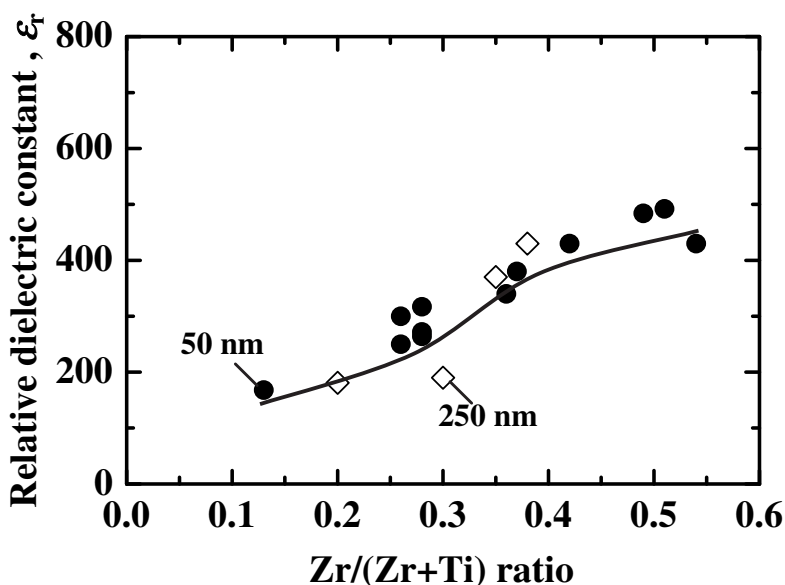Fig. 14. Evolution of ε_r measured at 1 kHz as function of Zr/(Zr+Ti) ratio for 50 nm (●) and 250 nm (◇) thick films.

On the other hand, we noticed that squareness in P - E hysteresis loops defined by the P_r/P_{sat} ratio, is also influenced by the Zr/(Zr+Ti) ratio of the films regardless of V_c in the film. [see Fig. 15 (a)]. Indeed, as it can be observed on this figure, both 50 nm and 250 nm thick films present the same decreasing trend when Zr/(Zr+Ti) ratio increases. This result is in a good agreement with results presented on Fig. 14 since ε_r can be extracted from the saturated branch of P - E hysteresis loops.
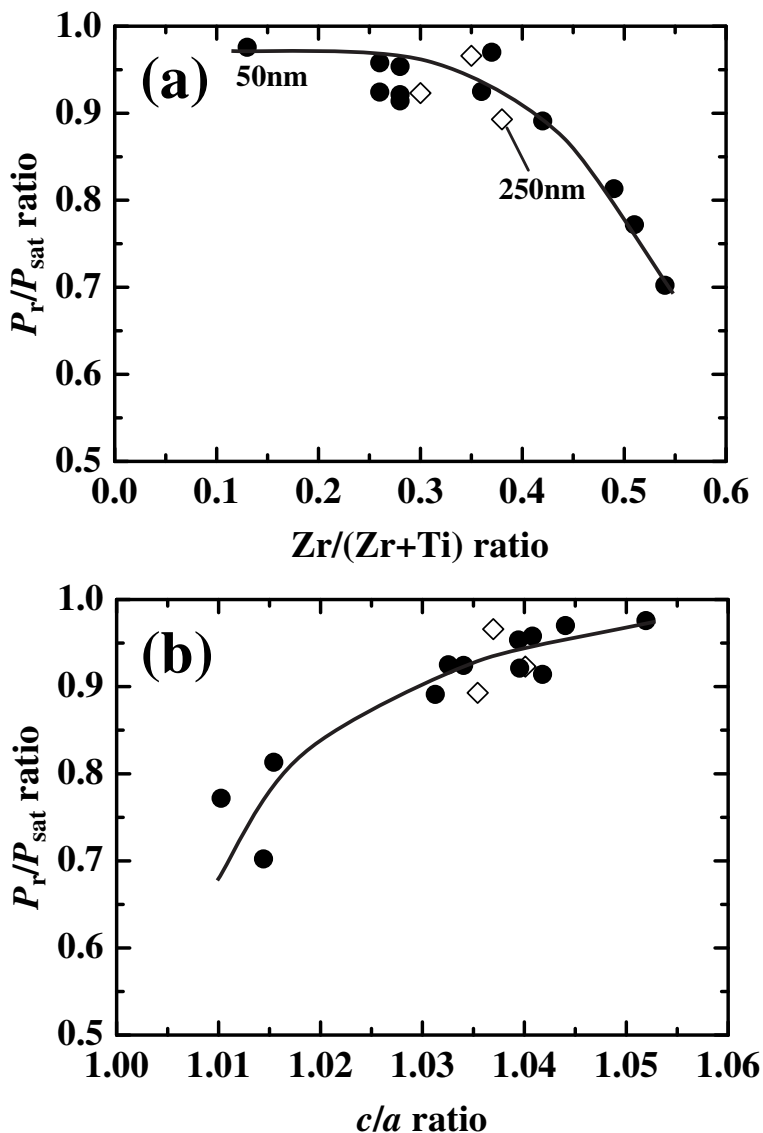
Fig. 15. Evolution of P_r/P_{sat} ratio as function of Zr/(Zr+Ti) ratio (a) and c/a ratio (b)

4. Summary

Epitaxial PZT thin films were grown at 540°C on SrRuO$_3$-coated (001) SrTiO$_3$ substrates by pulsed MOCVD. To characterize the impacts of the Zr/(Zr+Ti) ratio and the film thickness on the volume fraction of c-domain, 50 nm and 250 nm thick films have been grown with different Zr/(Zr+Ti) ratio ranging from 0.1 to 0.7.

HRXRD characterization showed that 50 nm thick films present a fully polar-axis oriented tetragonal films regardless of Zr/(Zr+Ti) up to 0.54, while 250 nm thick films are tetragonal single phase for the films with the Zr/(Zr+Ti) ratio smaller than 0.45, then, coexistence of tetragonal and rhombohedral phase from Zr/(Zr+Ti)=0.45 to 0.6. Appearing of two symmetry coexistence is related to the stress relaxation process occurring at relatively thick film.

Concerning electrical properties, 50-nm-thick PZT films with fully polar-axis orientation present larger P_r and P_{sat} values than thicker films. On the other hand, we investigated the impact of Zr/(Zr+Ti) ratio on the ferroelectricity of PZT films, showing the linear relationship between P_{sat}^2 and the c/a ratio of the films.

5. Acknowledgement

6. References

K. Nagashima, M. Aratani, and H. Funakubo, J. Appl. Phys. 89, 4517 (2001).

N. Okuda, K. Saito, and H. Funakubo, Jpn. J. Appl. Phys., Part 1 39, 572 (2000).

K. Saito, T. Kurosawa, T. Akai, T. Oikawa, and H. Funakubo, J. Appl. Phys. 93, 545 (2003).

G. Shirane and K. Suzuki, J. Phys. Soc. Jpn. 7, 333 (1952).

H. Morioka, S. Yokoyama, T. Oikawa, K. Saito and H. Funakubo. Mat. Res. Soc. Symp. Proc. 784, C6.2.1 (2004)

H. Morioka, S. Yokoyama, T. Oikawa and H. Funakubo Appl. Phys. Lett. 85, 3516 (2004).

K. Saito, T. Kurosawa, T. Akai, S. Yokoyama, H. Morioka, T. Oikawa, and H. Funakubo, Mater. Res. Soc. Symp. Proc. 748, U13.4 (2003).

H. Morioka, G. Asano, T. Oikawa, H. Funakubo, and K. Saito, Appl. Phys. Lett. 82, 4761 (2003).

H. Morioka, K. Saito, S. Yokoyama, T. Oikawa, T. Kurosawa, and H. Funakubo, J. Mater. Sci. 44, 5318 (2009)

T. Shiosaki, Science Forum, Japan (1995)

T. Oikawa, K. Takahashi, J. Ishida, Y. Ichikawa, T. Ochiai, K. Saito, A. Sawabe and H. Funakubo, Int. Ferro. 46, 55 (2002)

J. Ishida, T. Yamada, A. Sawabe, K. Okuwada, and K. Saito, Appl. Phys. Lett. 80, 467 (2002)

M. J. Haun, Z. Q. Zhuang, E. Furman, S. J. Jang, and L. E. Cross, J. Am. Ceram. Soc. 72, 1140 (1989)

F. Jona and G. Shirane, Ferroelectric Crystal, 145, Dover, New York, (1992).
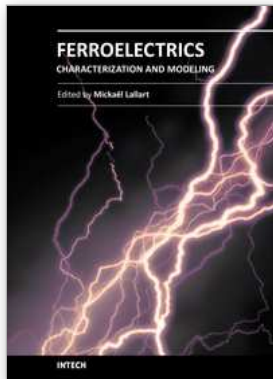
Ferroelectrics - Characterization and Modeling

Edited by Dr. Mickaël Lallart

Ferroelectric materials have been and still are widely used in many applications, that have moved from sonar towards breakthrough technologies such as memories or optical devices. This book is a part of a four volume collection (covering material aspects, physical effects, characterization and modeling, and applications) and focuses on the characterization of ferroelectric materials, including structural, electrical and multiphysic aspects, as well as innovative techniques for modeling and predicting the performance of these devices using phenomenological approaches and nonlinear methods. Hence, the aim of this book is to provide an up-to-date review of recent scientific findings and recent advances in the field of ferroelectric system characterization and modeling, allowing a deep understanding of ferroelectricity.

How to reference

In order to correctly reference this scholarly work, feel free to copy and paste the following:

Mohamed-Tahar Chentir, Hitoshi Morioka, Yoshitaka Ehara, Keisuke Saito, Shintaro Yokoyama, Takahiro Oikawa and Hiroshi Funakubo (2011). Changes of Crystal Structure and Electrical Properties with Film Thickness and Zr/(Zr+Ti) Ratio for Epitaxial Pb(Zr,Ti)O3 Films Grown on (100)cSrRuO3//(100)SrTiO3 Substrates by Metalorganic Chemical Vapor Deposition, Ferroelectrics - Characterization and Modeling, Dr. Mickaël Lallart (Ed.), ISBN: 978-953-307-455-9, InTech, Available from:

http://www.intechopen.com/books/ferroelectrics-characterization-and-modeling/changes-of-crystal-structure-and-electrical-properties-with-film-thickness-and-zr-zr-ti-ratio-for-ep

INTECH
open science | open minds